Nanoscale

COMMUNICATION

View Article Online
View Journal | View Issue

Cite this: *Nanoscale*, 2021, **13**, 11343

Received 17th May 2021,
Accepted 21st June 2021

DOI: 10.1039/d1nr03170h

rsc.li/nanoscale

Communicating assemblies of biomimetic nanocapsules†

Hongda Zhou,[a] Haowei Huang,[a,b] Mounib Bahri,[c] Nigel D. Browning,[c] James Smith,[a] Michael Graham[a] and Dmitry Shchukin *[a]

Communication assemblies between biomimetic nanocapsules in a 3D closed system with self-regulating and self-organization functionalities were demonstrated for the first time. Two types of biomimetic nanocapsules, TiO_2/polydopamine capsules and SiO_2/polyelectrolytes capsules with different stimuli-responsive properties were prepared and leveraged to sense the external stimulus, transmit chemical signaling, and autonomic communication-controlled release of active cargos. The capsules have clear core–shell structures with average diameters of 30 nm and 25 nm, respectively. The nitrogen adsorption–desorption isotherms and thermogravimetric analysis displayed their massive pore structures and encapsulation capacity of 32% of glycine pH buffer and 68% of benzotriazole, respectively. Different from the direct release mode of the single capsule, the communication assemblies show an autonomic three-stage release process with a "jet lag" feature, showing the internal modulation ability of self-controlled release efficiency. The control overweight ratios of capsules influences on communication-release interaction between capsules. The highest communication-release efficiency (89.6% of benzotriazole) was achieved when the weight ratio of TiO_2/polydopamine/SiO_2/polyelectrolytes capsules was 5 : 1 or 10 : 1. Communication assemblies containing various types of nanocapsules can autonomically perform complex tasks in a biomimetic fashion, such as cascaded amplification and multidirectional communication platforms in bioreactors.

Introduction

Biological regulatory networks use chemical signaling molecules to drive cell communications and coordinate their actions to obtain quorum-based functionalities.[1–3] Communicating behaviors play a pivotal role in self-organizing processes across all-natural objects, from single cells to individual organisms. For instance, signaling molecules can be recognized by the cellular membrane and transmitted to the genome;[4,5] bacteria release autoinducers communicate with other individuals through processes like quorum sensing.[6,7] The cell-to-cell communication in natural bacteria is the most typical and has been studied extensively. The cell-to-cell interactions involve producing, releasing, detecting, and responding. Recognition of the triggers, chemical signals, receptors, target genes, and mechanisms of signal transduction is leading to a comprehensive understanding of communication between cells.[8] Communicating behaviors between artificial materials and bacterial cells have received considerable attention during the last years.[9–12] Theoretical and computational models have demonstrated communication ability caused by chemical signaling.[13–15] However, according to our best knowledge, there is no wholly artificial biomimetic system that can represent or simulate the process of generating, transforming, and processing chemical signals.

Biomimetic nanocapsules have been of great interest in a wide range of scientific areas such as drug delivery,[16,17] catalysis,[18,19] analytical applications,[20] self-healing coatings[21] and multifunctional autonomic materials.[22] Nanocapsules consisting of hollow or porous structures can encapsulate various active cargos (*e.g.*, drugs, enzymes, biocides). The nanocapsules have a shell that isolates the encapsulated material from the surrounding environment and has controlled release properties of the cargo. Generally, nanocapsules' fabrication requires the loading of active cargo and the formation of a stable shell with controlled permeability.[23] Over the last couple of years, various smart materials (*e.g.*, nanoparticles, polymers, proteins) have been introduced for the formation of capsule shells.[24–26] Types of stimuli strategies have also been designed in many research works to trigger reversible or irreversible shell transformations/deformation such as pH change,[27] ionic strength,[28] light,[29] and ultrasonication.[30,31] However, all of them focus on individual capsules reacting to external environmental stimuli. There are no examples of two

[a]*Stephenson Institute for Renewable Energy and Department of Chemistry, University of Liverpool, Liverpool, L69 7ZD, UK. E-mail: d.shchukin@liverpool.ac.uk*
[b]*School of Chemistry and Chemical Engineering, South China University of Technology, Guangzhou, 510640, China*
[c]*Albert Crewe Centre, University of Liverpool, Liverpool, L69 3GL, UK*
†Electronic supplementary information (ESI) available. See DOI: 10.1039/d1nr03170h

or more different capsules cooperating with each other as well as no mentioning of the capsules' behavior in communicating assemblies.

Artificially designed assemblies of biomimetic nanocapsules will play a significant role in a new generation of smart materials, which enables precise temporal control in a 3D environment and reproducing natural events during material exploitation. Inspired by the biological regulatory networks, we propose a strategy for the rational design of programmable functional assemblies of biomimetic nanocapsules. Compared with a single capsule, these assemblies allow different capsules to work cooperatively achieving complicated and versatile functions. Among these assemblies, the single capsule can sense the external environment changes, and, by releasing initiating cargo, chemically inform surrounding capsules for their further active response. The assemblies of communicating biomimetic nanocapsules can exhibit self-regulating, self-organization functionalities involving internal modulation ability of self-controlled release rate. We built a capsule community containing two types of nanocapsules that exhibit dynamic behavior by chemical information exchange between capsules (Fig. 1). One type is TiO_2/polydopamine hybrid capsules (TiO_2–pH@PDA) with encapsulated initiating cargo (pH buffer glycine) as a core which release can be triggered by visible light, and nanostructured hybrid shell containing TiO_2 and polydopamine. The other, receptor-like type, is SiO_2/polyelectrolytes composite capsules, which are pH-responsive and contain active agents (*e.g.*, benzotriazole, BTA) as a core and composite shell formed by SiO_2 and multilayered polyelectrolyte layers (SiO_2–BTA@PEs). The communicating behavior and chemical mechanisms of the assemblies in a 3D environment have been investigated. The knowledge gained from these artificial capsule networks may lead to the design of synthetic systems that can perform complex tasks in a biomimetic fashion. It will also provide the route to create platforms and devices with self-recognition and self-regulating functionalities without continuous external impact.

Results and discussion

Two types of inorganic nanospheres (TiO_2 and SiO_2) were synthesized using reverse microemulsions as templates to obtain nanocapsules with large interior space and developed pore structures. Also, the robust inorganic nanospheres allow the high loading of cargo inside the capsule. DLS analysis indicates that the as-synthesized TiO_2 and SiO_2 nanospheres are monodisperse with average hydrodynamic diameters of 20 ± 5 nm and 18 ± 5 nm, respectively. After exterior shell formation, the final capsules with cargo have average hydrodynamic diameters of 30 ± 5 nm and 25 ± 5 nm, respectively (Fig. S1†). With polydopamine decoration, TiO_2 nanospheres have a broader size distribution, caused by polydopamine strong adhesion to TiO_2. However, the SiO_2 nanospheres with multilayered polyelectrolytes have a narrow size distribution, owing to the electrostatic repulsion between poly (sodium 4-styrenesulfonate) (PSS) used as final polyelectrolyte layer. Transmission electron microscopy (TEM) analysis was performed to observe inorganic nanospheres' morphology and structure before and after encapsulation (Fig. 2). From the images, it can be noted that both TiO_2–pH@PDA and SiO_2–BTA@PEs capsules have clear core–shell structure after encapsulation.

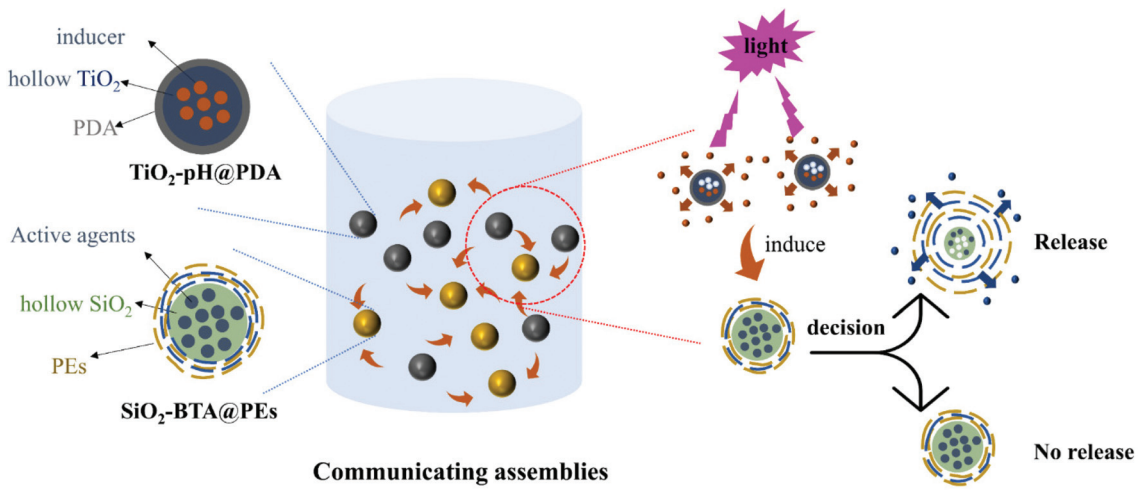

Fig. 1 Schematic representation of the self-controlled artificial nanocapsule networks. Stable reverse microemulsion templates were first prepared by mixing cyclohexane, deionized water, and non-ionic surfactant polyoxyethylene nonylphenylether (CO-520). The as-formed microemulsion was ultrasonicated for 15 min to obtain uniform and monodisperse droplets, followed by growing inorganic shells (TiO_2/SiO_2) on the templates. Subsequently, the formation of biomimetic nanocapsules was present by cargo loading and exterior shell building through dopamine polymerisation and polyelectrolyte layer-by-layer (LBL) assembly, respectively. Then, the mixed solution containing TiO_2–pH@PDA and SiO_2–BTA@PEs was illuminated by visible light for 400 min using a 100 W Xe lamp under continuous stirring. The pH change of the solution was tested at the given interval. The fluorescence intensity at the emission maximum of BTA was plotted as a function of time to obtain a final communication-controlled release profile.

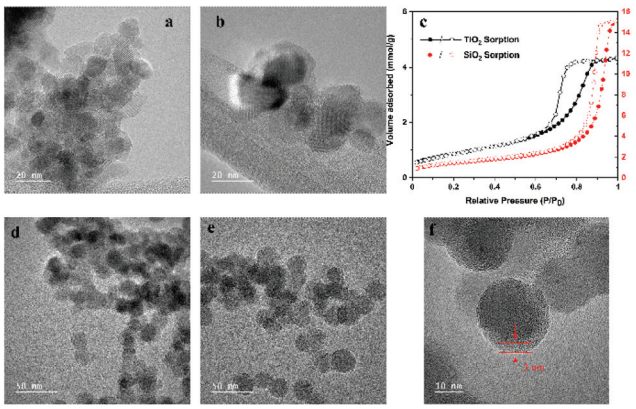

Fig. 2 TEM image of a typical (a) TiO_2; (b) TiO_2–pH@PDA capsules; (c) N_2 sorption isotherms of TiO_2 and SiO_2 (77.3 K): (i) filled circles, adsorption experiments; (ii) unfilled circle, desorption experiments. (d) TEM images of SiO_2; and (e) SiO_2–BTA@PEs capsules; (f) the enlarged view of a single SiO_2–BTA@PEs capsule.

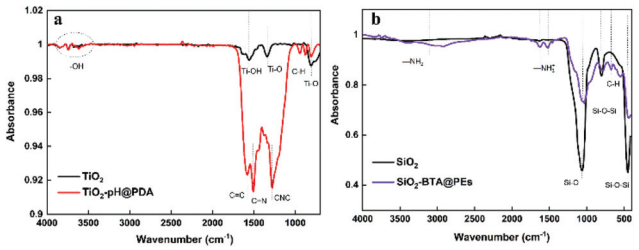

Fig. 3 ATR-FTIR spectra of (a) TiO_2 (black), TiO_2–pH@PDA capsules (red); (b) SiO_2 (black), SiO_2–BTA@PEs capsules (purple).

The nitrogen adsorption–desorption isotherms were measured to characterize the pore structures of as-synthesized TiO_2 and SiO_2 nanospheres (Fig. 2c). According to the IUPAC classification,[32] both isotherms are classic type IV showing a hysteresis loop characteristic to mesoporous materials. For the TiO_2 nanospheres, the curve exhibits a hysteresis type $_2$ loop at the relative pressures between 0.6 and 0.8. It is well known that various size of the cavities causes this type of hysteresis loop. This result indicated that TiO_2 nanospheres have massive disordered mesopores structure. The massive mesopore structure has lots of ink-bottle shapes with narrow necks and broader bodies providing huge cavities for cargo encapsulation.

The SiO_2 nanospheres have a narrower hysteresis loop and almost parallel hysteresis branches. It is confirmed that the SiO_2 nanospheres have a highly homogeneous interconnected 3D mesopore structure with large, well-ordered mesopores. The proper interior structure of inorganic nanospheres benefits the maximum loading of different cargos. Thermogravimetric analysis (TGA) demonstrated the maximum encapsulation capacity for both nanospheres (Fig. S2†). The final TiO_2–pH@PDA and SiO_2–BTA@PEs capsules possess the maximum loading of cargos for 32% and 68%, respectively. The detailed structural information of both capsules is illustrated in Table 1 for comparison.

To further confirm the formation of hybrid nanocapsules, the chemical composition of the initial inorganic nanospheres and final encapsulated nanocapsules was characterized by attenuated total reflection-Fourier transform infrared (ATR-FTIR) spectroscopy (Fig. 3). A series of weak absorption peaks at about 3500 cm^{-1} can be attributed to the stretching vibration of the –OH bond. The peak at 1630 cm^{-1} is assigned to the bonding modes of Ti–OH. The typical absorption peaks at 630 and 1380 cm^{-1} are corresponding to the stretching vibration of Ti–O. Compared with the TiO_2, the TiO_2–pH@PDA capsules show extra absorption peaks at 1060, 1250, 1502, and 1640 cm^{-1} which can be assigned to the bending δ(C–H), the indole ring CNC stretching, ν_{ring}(C═N) stretching, and ν_{ring}(C═C) stretching modes (Fig. 3a). The spectra profile of SiO_2–BTA@PEs capsules also provides series of characteristic peaks. The absorption peaks at 475, 820, and 1098 cm^{-1} can be attributed to Si–O–Si bending vibration, symmetric stretching of Si–O–Si, and asymmetric vibration of Si–O. After encapsulation, a small peak at 750 cm^{-1} is found, which corresponds to in-plane bending vibrations of C–H in the BTA benzene ring. Also, the peaks at 1470 and 1590 cm^{-1} can be assigned to the symmetric distortion and asymmetric stretching vibrations of $-NH^{3+}$. The peaks of hydrogen bonding caused by C–H vibration can be found at about 2840–2990 cm^{-1}. Also, two weak peaks at 3150 and 3400 cm^{-1} correspond to the $-N_2$ group (Fig. 3b). The ATR-FTIR analysis indicated that the polydopamine and multilayered PEs successfully decorated the surface of TiO_2 and SiO_2, respectively.

In order to study the release kinetics of a single capsule, we carried out photodegradation measurement and BTA release curve test on individual TiO_2–pH@PDA capsules and SiO_2–BTA@PEs capsules first. The detailed experimental procedures and methods can be found in ESI.† For the light-responsive TiO_2–pH@PDA capsules, the stimuli-release performance was tested by pH change of the solution and photocatalytic activity through degrading of Rhodamine B (RhB) under visible light irradiation. Typically, pristine TiO_2 can respond to UV irradiation but shows no photoactivity under visible light irradiation. Hence, we employed PDA as a surface modifier to obtain TiO_2–pH@PDA hybrid shell sensitivity to visible light.

Table 1 Structures and properties of TiO_2–pH@PDA and SiO_2–BTA@PEs capsules

Sample	Nanosphere size (nm)	Capsule size (nm)	Surface area ($cm^2\ g^{-1}$)	Pore volume ($cm^3\ g^{-1}$)	Encapsulation capacity (%)
TiO_2–pH@PDA capsules	20 ± 5	30 ± 5	97.07	0.15	32
SiO_2–BTA@PEs capsules	18 ± 5	25 ± 5	161.47	0.42	68

The improved photoactivity of TiO_2–pH@PDA capsules was confirmed by the complete degradation of RhB (wavelength = 560 nm) after 180 min of visible light irradiation (Fig. S3†). The release of pH buffer from TiO_2–pH@PDA was tested under visible light irradiation at continuous stirring (Fig. S4†). The pH value increased gradually and reached equilibrium after 220 min of irradiation. However, the suspension pH was kept almost unchanged without visible light irradiation. Therefore, PDA modification can effectively suppress spontaneous leakage from TiO_2 mesopores and provide effective light-response in the visible light range.

The layer-by-layer (LBL) technique is a well-studied method to fabricate microcapsules. The release profile of BTA from SiO_2–BTA@PEs capsules was measured at different pH (Fig. S5†). The variation of BTA adsorption peaks (274 nm) *versus* time is shown in Fig. S6.† The multi-layered polyelectrolyte shells composed of weak polyelectrolytes (PAH and PSS) are responsive to the pH of the environment. The leakage of BTA was restrained by multilayered polyelectrolytes at pH = 7. When pH increases to 10, the multi-layered polyelectrolytes will swell to increase the permeability, BTA molecules demonstrate a gradual release process. About 35% of BTA was released in the first 20 min.

After revealing the stimuli-responsive behaviour of single capsules alone, we focused on the internal communication between different capsules in a solution. The nanosized capsules containing different chemical signalling and cargos were mixed in an aqueous solution under stirring. The pH buffer (pH = 10) encapsulated inside the TiO_2–pH@PDA capsules was introduced as a chemical signal to build the communication bridge between two different types of capsules. After the TiO_2–pH@PDA was initiated by light exposure, the pH buffer was released as exchanging substances to the solution leading to the pH change. The SiO_2–BTA@PEs subsequently response to the pH change and finish the communication-controlled BTA release. Fig. 4a shows the typical spectrum of communication-controlled BTA release (TiO_2–pH@PDA/SiO_2–BTA@PEs = 5 : 1 mixing ratio). The adsorption peak of BTA has a noticeable increase with the time increased. This indicates that the release of BTA, which is not controlled by light in SiO_2–BTA@PEs capsules, is controlled by light now in the presence of TiO_2–pH@PDA capsules. This is owed to TiO_2–pH@PDA, which can regulate the pH of the closed system acting as a signal bridge. Compared with the direct release mode of BTA (solution pH = 10) from SiO_2–BTA@PEs capsules, the communication-controlled release has an entirely different release mode (Fig. 4b).

We revealed three periods of the whole autonomic communication-controlled release process. At the first stage (0–180 min), a slow-release profile is caused by the slight pH change and a low release of BTA was observed. Subsequently, more pH buffer was released from the TiO_2–pH@PDA under continuous visible light irradiation at 180–280 min period leading to the faster release of BTA at the second stage. The maximum release efficiency (89.6%) was achieved at the end of release process (280–400 min). It is worth noting that the communication system shows a "jet lag" between pH change and BTA release.

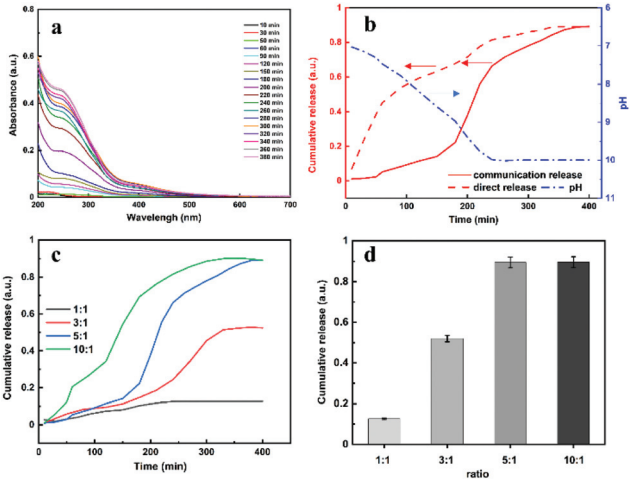

Fig. 4 Dynamic release behaviour controlled by chemical information exchange between different capsules. (a) UV-vis spectra of BTA released from SiO_2–BTA@Pes capsules (TiO_2–pH@PDA/SiO_2–BTA@PEs = 5 : 1); (b) the release profile of BTA controlled by single SiO_2–BTA@PEs capsules (red dotted line) and communication-controlled by mixed capsules (red line), and pH change (blue line); (c) the release profile of BTA under different ratio of TiO_2–pH@PDA to SiO_2–BTA@Pes capsules; (d) the cumulative release efficiency of BTA under different ratio of TiO_2–pH@PDA to SiO_2–BTA@Pes capsules.

In principle, the multilayered PSS/PAH shell is open at pH = 10. However, the BTA release rate started to increase at about pH = 9.5. Typically, BTA is an amphoteric compound and benzotriazole species can be transferred through protonic equilibria depending on the solution pH. Under a basic environment (pH = 10), the neutral benzotriazole becomes deprotonated with local OH– consumption leading to the initial delay phenomenon by decreasing free OH– concentration. Before the pH change to 10 (first 200 min), the release efficiency of BTA is about 18%. This evidences that when SiO_2–BTA@PEs capsules received chemical signals sent by TiO_2–pH@PDA, they can either release cargos or not respond depending on OH– concentration.

The communication behavior can also be affected by the weight ratio of TiO_2–pH@PDA/SiO_2–BTA@PEs mixture (Fig. 4c and d). The study of communication release behaviour under different ratios was illustrated in Fig. S7.† When the ratio is 1 : 1, there is almost no communication observed between capsules. The quantity of pH buffer released from TiO_2–pH@PDA capsules is not enough to change the solution pH to 10 because all OH– is consumed by the deprotonated benzotriazole. When the ratio increases to 3 : 1, more pH buffer diffuses into the external solution. The shell of SiO_2–BTA@PEs capsules was opened after 220 min of irradiation, the release efficiency is gradually increased for about 60 min and then reached a final equilibrium of 50%. Although SiO_2–BTA@PEs capsules were opened, there is not enough encapsulated pH buffer to reach protonic equilibrium. The existed OH– is con-

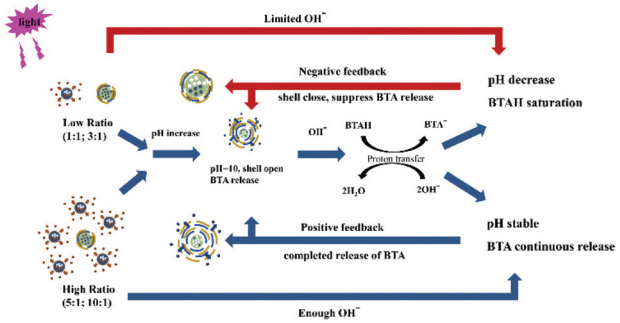

Fig. 5 Schematic representation of the communication mechanism of self-controlled artificial nanocapsule networks. The different weight ratios of TiO_2–pH@PDA/SiO_2–BTA@PEs capsules create different self-communication strategy. The lower ratio leads to incomplete release of BTA with a negative feedback loop. The higher ratios trigger complete release of BTA with positive feedback loop.

tinuously consumed by BTA, leading to the pH decrease. So, the multi-layered polyelectrolytes shells are closing again after 50% BTA release. The neutral benzotriazole concentration in the solution also reaches saturation level suppressing the continuous release of BTA from SiO_2–BTA@PEs capsules and creating stopping feedback response. The communication behavior between capsules stops due to the lack of chemical signals, and the final incomplete release of BTA is achieved. The maximum release efficiency is obtained at the 5 : 1 or 10 : 1 TiO_2–pH@PDA/SiO_2–BTA@PEs weight ratio. Sufficient amount of pH buffer triggers intensive release of BTA with positive feedback.[33] (Fig. 5). The abundant pH buffer supply keeps the pH stable during BTA protonation process. The polyelectrolytes shell is open and BTA is continuously released and deprotonated, leading the completed BTA release. By this way, we achieved biomimetic reproduction of the effective chemical signal cooperations between biological cells.

The different nanocapsules containing pH buffer and BTA were mixed in an aqueous solution to make complete autonomic signalling system. Hence, considering the dynamic stimuli-response-communication-decide-response behavior, the assemblies of different biomimetic nanocapsules can exhibit self-regulating, self-organization functionalities involving internal modulation of self-controlled release efficiency.

Conclusions

In summary, we have successfully demonstrated autonomic communications between different nanocapsules in one system. This provides the possibility of self-regulating and self-organization functionalities and finally shifts control from external stimuli to internal chemical communication between capsules. The colonies of different capsules can exhibit more complicated functions by incorporating communication shuttles and internal modulation ability. We believe such a rational design idea would lead to the development of synthetic systems that can perform autonomic complex tasks in a biomimetic fashion. Also, the combination of uniquely response behaviour and communication opens up exciting opportunities in the design of soft functional materials that are capable of signal transduction. For example, a wide variety of biomimetic communication platforms capable of cascaded amplification and bidirectional communication can be introduced. Or, soft robotic materials have to depend on the ability to exchange signals and react upon them often in complex environments. Furthermore, different inducers and cargos can be encapsulated inside the capsules to realize more complicated autonomic applications, from biological technology to materials science. It can even provide internal physiological cycle changes for the robotic systems.

Author contributions

Hongda Zhou: Investigation. Haowei Huang: Investigation. Mounib Bahri: Visualization. Nigel D. Browning: Validation. James Smith: Investigation. Michael Graham: Investigation. Dmitry Shchukin: Supervision.

Conflicts of interest

There are no conflicts to declare.

Acknowledgements

This work was supported by ERC Consolidator project ENERCAPSULE (grant 647969) and RSC International Exchanges grant IEC/R2/202163. H. Zhou thanks the China Scholarship Council for a PhD studentship. The TEM experiments were performed in the Albert Crewe Centre (ACC) for Electron Microscopy at the University of Liverpool, a Shared Research Facility supported by the Faculty of Science and Engineering.

References

1 M. S. Sundrud, S. B. Koralov, M. Feuerer, D. P. Calado, A. E. Kozhaya, A. Rhule-Smith, R. E. Lefebvre, D. Unutmaz, R. Mazitschek, H. Waldner, M. Whitman, T. Keller and A. Rao, *Science*, 2009, **324**, 1334–1338.
2 N. Yosef, A. K. Shalek, J. T. Gaublomme, H. Jin, Y. Lee, A. Awasthi, C. Wu, K. Karwacz, S. Xiao, M. Jorgolli, D. Gennert, R. Satija, A. Shakya, D. Y. Lu, J. J. Trombetta, M. R. Pillai, P. J. Ratcliffe, M. L. Coleman, M. Bix, D. Tantin, H. Park, V. K. Kuchroo and A. Regev, *Nature*, 2013, **496**, 461–468.
3 M. R. Hepworth, L. A. Monticelli, T. C. Fung, C. G. K. Ziegler, S. Grunberg, R. Sinha, A. R. Mantegazza, H. L. Ma, A. Crawford, J. M. Angelosanto, E. John Wherry, P. A. Koni, F. D. Bushman, C. O. Elson, G. Eberl, D. Artis and G. F. Sonnenberg, *Nature*, 2013, **498**, 113–117.
4 H. Jung, B. C. Yoon and C. E. Holt, *Nat. Rev. Neurosci.*, 2012, **13**, 308–324.

5 P. Zhang, X. Han, J. Yao, N. Shao, K. Zhang, Y. Zhou, Y. Zu, B. Wang and L. Qin, *Angew. Chem., Int. Ed.*, 2019, **58**, 13700–13705.
6 X. Chen, S. Schauder, N. Potier, A. Van Dorsselaer, I. Pelczer, B. L. Bassler and F. M. Hughson, *Nature*, 2002, **415**, 545–549.
7 W.-L. Ng and B. L. Bassler, *Annu. Rev. Genet.*, 2009, **43**, 197–222.
8 C. M. Waters and B. L. Bassler, *Annu. Rev. Cell Dev. Biol.*, 2005, **21**, 319–346.
9 R. Lentini, S. P. Santero, F. Chizzolini, D. Cecchi, J. Fontana, M. Marchioretto, C. Del Bianco, J. L. Terrell, A. C. Spencer, L. Martini, M. Forlin, M. Assfalg, M. D. Serra, W. E. Bentley and S. S. Mansy, *Nat. Commun.*, 2014, **5**, 1–6.
10 H. Kang, H. J. Jung, D. S. H. Wong, S. K. Kim, S. Lin, K. F. Chan, L. Zhang, G. Li, V. P. Dravid and L. Bian, *J. Am. Chem. Soc.*, 2018, **140**, 5909–5913.
11 P. M. Gardner, K. Winzer and B. G. Davis, *Nat. Chem.*, 2009, **1**, 377–383.
12 A. Zargar, D. N. Quan, N. Abutaleb, E. Choi, J. L. Terrell, G. F. Payne and W. E. Bentley, *Biotechnol. Bioeng.*, 2017, **114**, 407–415.
13 J. S. Coggan, T. M. Bartol, E. Esquenazi, J. R. Stiles, S. Lamont, M. E. Martone, D. K. Berg, M. H. Ellisman and T. J. Sejnowski, *Science*, 2005, **309**, 446–451.
14 P. Dayal, O. Kuksenok and A. C. Balazs, *Proc. Natl. Acad. Sci. U. S. A.*, 2013, **110**, 431–436.
15 O. Kuksenok, P. Dayal, A. Bhattacharya, V. V. Yashin, D. Deb, I. C. Chen, K. J. Van Vliet and A. C. Balazs, *Chem. Soc. Rev.*, 2013, **42**, 7257–7277.
16 P. Sahandi Zangabad, M. Karimi, F. Mehdizadeh, H. Malekzad, A. Ghasemi, S. Bahrami, H. Zare, M. Moghoofei, A. Hekmatmanesh and M. R. Hamblin, *Nanoscale*, 2017, **9**, 1356–1392.
17 A. Vonarbourg, C. Passirani, L. Desigaux, E. Allard, P. Saulnier, O. Lambert, J. P. Benoit and B. Pitard, *Biomaterials*, 2009, **30**, 3197–3204.
18 C. Wang, X. Jie, Y. Qiu, Y. Zhao, H. A. Al-Megren, S. Alshihri, P. P. Edwards and T. Xiao, *Appl. Catal., B*, 2019, **259**, 118019.
19 G. Cai, M. Ding, Q. Wu and H.-L. Jiang, *Natl. Sci. Rev.*, 2020, **7**, 37–45.
20 C. Hofmann, A. Duerkop and A. J. Baeumner, *Angew. Chem., Int. Ed.*, 2019, **58**, 12840–12860.
21 D. Borisova, H. Möhwald and D. G. Shchukin, *ACS Appl. Mater. Interfaces*, 2013, **5**, 80–87.
22 E. Shchukina and D. G. Shchukin, *Langmuir*, 2019, **35**, 8603–8611.
23 H. Gao, D. Wen, N. V. Tarakina, J. Liang, A. J. Bushby and G. B. Sukhorukov, *Nanoscale*, 2016, **8**, 5170–5180.
24 F. Caruso, *Chem. – Eur. J.*, 2000, **6**, 413–419.
25 A. J. Jadhav, D. V. Pinjari and A. B. Pandit, *Chem. Eng. J.*, 2016, **297**, 116–120.
26 G. Chen, A. A. Abdeen, Y. Wang, P. K. Shahi, S. Robertson, R. Xie, M. Suzuki, B. R. Pattnaik, K. Saha and S. Gong, *Nat. Nanotechnol.*, 2019, **14**, 974–980.
27 B. Qian, Z. Zheng, M. Michailids, N. Fleck, M. Bilton, Y. Song, G. Li and D. Shchukin, *ACS Appl. Mater. Interfaces*, 2019, **11**, 10283–10291.
28 K. Köhler, D. G. Shchukin, H. Möhwald and G. B. Sukhorukov, *J. Phys. Chem. B*, 2005, **109**, 18250–18259.
29 J. Borges, L. C. Rodrigues, R. L. Reis and J. F. Mano, *Adv. Funct. Mater.*, 2014, **24**, 5624–5648.
30 D. G. Shchukin, D. A. Gorin and H. Möhwald, *Langmuir*, 2006, **22**, 7400–7404.
31 M. Gai, J. Frueh, T. Tao, A. V. Petrov, V. V. Petrov, E. V. Shesterikov, S. I. Tverdokhlebov and G. B. Sukhorukov, *Nanoscale*, 2017, **9**, 7063–7070.
32 M. D. Donohue and G. L. Aranovich, *Adv. Colloid Interface Sci.*, 1998, **76–77**, 137–152.
33 C. Djugnat and G. B. Sukhorukov, *Langmuir*, 2004, **20**, 7265–7269.